AD_____

GRANT NUMBER DAMD17-96-1-6200

TITLE: A Dedicated PET Scanner for Axillary Node Imaging

PRINCIPAL INVESTIGATOR: Simon Cherry, Ph.D.

CONTRACTING ORGANIZATION: University of California, Los Angeles
Los Angeles, CA 90095-1406

REPORT DATE: September 1998

TYPE OF REPORT: Final

PREPARED FOR: Commander
U.S. Army Medical Research and Materiel Command
Fort Detrick, Frederick, Maryland 21702-5012

REPORT DOCUMENTATION PAGE

Form Approved
OMB No. 0704-0188

1. AGENCY USE ONLY *(Leave blank)*	2. REPORT DATE	3. REPORT TYPE AND DATES COVERED
	September 1998	Final (1 Sep 96 - 31 Aug 98)

4. TITLE AND SUBTITLE
A Dedicated PET Scanner for Axillary Node Imaging

5. FUNDING NUMBERS
DAMD17-96-1-6200

6. AUTHOR(S)
Simon Cherry, Ph.D.

7. PERFORMING ORGANIZATION NAME(S) AND ADDRESS(ES)
University of California, Los Angeles
Los Angeles, CA 90095-1406

8. PERFORMING ORGANIZATION REPORT NUMBER

9. SPONSORING/MONITORING AGENCY NAME(S) AND ADDRESS(ES)
Commander
U.S. Army Medical Research and Materiel Command
Fort Detrick, Frederick, Maryland 21702-5012

10. SPONSORING/MONITORING AGENCY REPORT NUMBER

11. SUPPLEMENTARY NOTES

12a. DISTRIBUTION / AVAILABILITY STATEMENT
Approved for public release; distribution unlimited

12b. DISTRIBUTION CODE

13. ABSTRACT *(Maximum 200*

A key prognostic factor in breast cancer is the involvement of the axillary lymph nodes. This is currently determined by axillary lymph node dissection (ALND), a low yield surgical procedure associated with significant cost and morbidity. Positron Emission Tomography (PET), using [F-18]fluorodeoxyglucose (FDG) tracer is a sensitive and non-invasive test for lymph node involvement and can be a cost effective alternative to ALND. In this project we have developed a low cost, high performance dedicated PET camera (maxPET) for axillary node imaging. The system can also be used for direct imaging of the breast.

The system consists of two 9 x 9 cm area planar scintillation detector arrays, comprising 3x3x20 mm lutetium oxyorthosilicate (LSO) detector elements, read out by a 3 x 3 array of position sensitive photomultiplier tubes. We are currently assembling the system and developing the data acquisition hardware and software. The finished system is projected to have a spatial resolution of approximately 3 mm and a sensitivity of up to 40% for a central point source.

We have also developed a realistic phantom of the human torso for testing this system and other dedicated PET systems designed for breast cancer applications.

14. SUBJECT TERMS	15. NUMBER OF PAGES
Breast Cancer	19
	16. PRICE CODE

17. SECURITY CLASSIFICATION OF REPORT	18. SECURITY CLASSIFICATION OF THIS PAGE	19. SECURITY CLASSIFICATION OF ABSTRACT	20. LIMITATION OF ABSTRACT
Unclassified	Unclassified	Unclassified	Unlimited

FOREWORD

Opinions, interpretations, conclusions and recommendations are those of the author and are not necessarily endorsed by the U.S. Army.

____ Where copyrighted material is quoted, permission has been obtained to use such material.

____ Where material from documents designated for limited distribution is quoted, permission has been obtained to use the material.

SRC Citations of commercial organizations and trade names in this report do not constitute an official Department of Army endorsement or approval of the products or services of these organizations.

____ In conducting research using animals, the investigator(s) adhered to the "Guide for the Care and Use of Laboratory Animals," prepared by the Committee on Care and use of Laboratory Animals of the Institute of Laboratory Resources, national Research Council (NIH Publication No. 86-23, Revised 1985).

____ For the protection of human subjects, the investigator(s) adhered to policies of applicable Federal Law 45 CFR 46.

____ In conducting research utilizing recombinant DNA technology, the investigator(s) adhered to current guidelines promulgated by the National Institutes of Health.

____ In the conduct of research utilizing recombinant DNA, the investigator(s) adhered to the NIH Guidelines for Research Involving Recombinant DNA Molecules.

____ In the conduct of research involving hazardous organisms, the investigator(s) adhered to the CDC-NIH Guide for Biosafety in Microbiological and Biomedical Laboratories.

9/21/98

PI - Signature Date

TABLE OF CONTENTS

INTRODUCTION

Axillary lymph node involvement is the most important prognostic factor determining survival in patients with breast cancer. For this reason, virtually all these patients undergo axillary lymph node dissection (ALND), a surgical procedure which allows pathological examination of the nodes [1]. Unfortunately, ALND is associated with high cost and significant morbidity. In women receiving partial mastectomies, it is most commonly performed as a separate procedure, requiring hospitalization, general anesthesia and one to two weeks of post-operative drain care. Complications from this procedure include post-operative seroma formation, arm and breast edema, nerve injuries and shoulder dysfunction.

As a result of the introduction of screening programs and improvements in mammography, many breast cancers are being discovered at an earlier stage, and for this reason, the rate for positive findings during ALND procedures has dropped to as little as 25% [2]. Furthermore, earlier detection and changes in the management of breast carcinoma have resulted in a large increase in the number of women electing breast conservation therapy, where a partial mastectomy is combined with local radiation therapy. Partial mastectomies can be performed on an outpatient basis and do not require hospitalization. The value of an accurate, non-invasive test for axillary lymph node involvement is therefore clear. It would eliminate the need of hospitalization for tens of thousands of women and avoid the costs and morbidity associated with the surgical dissection of the axillary nodes.

Possible non-invasive tests include clinical examination and X-ray computed tomography. Both of these techniques have failed to show the necessary sensitivity to be considered as a replacement to the surgical ALND procedure [1,3-4]. However, a multi-center study using positron emission tomography (PET), with 2-[F-18]-fluoro-2-deoxy-D-glucose (FDG) as the tracer, demonstrated a sensitivity and specificity of 96% [2,5-9]. The average uptake in axillary metastases ranges from 2:1 to 30:1 relative to normal surrounding tissue [5]. These studies were carried out in conventional whole-body PET scanners. The same group showed, using conservative estimates, that by using PET instead of ALND in patients who were candidates for breast conservation therapy, the economic savings would be in excess of 50 million dollars a year. In addition, more than 70,000 women a year would have been spared ALND and its associated complications. These figures are for the United States alone.

Despite this very encouraging data, there are still two barriers which serve to hinder the widespread application of PET as a non-invasive test for axillary lymph node involvement. Firstly, according to the data, 3% of women with axillary node involvement are likely to be misclassified by PET. In general, these will be women who have less extensive lymph node involvement which the current generation of clinical PET scanners lack the sensitivity and spatial resolution to detect. Although this is regarded as an acceptable trade-off, since for every patient misclassified, 33 patients will have been spared the cost and morbidity of ALND, improvements in the sensitivity of PET techniques would be welcomed. A more practical aspect is related to the availability of PET instrumentation itself. Modern clinical PET scanners are extremely expensive and there are only approximately 40 PET scanners in the United States. It is unrealistic that these centers could scan 70,000 patients a year, and the geographic distribution of the scanners does not necessarily reflect the distribution of the patients.

To address both these issues, we are developing a small dedicated PET scanner for axillary node imaging. This system is designed to be an order of magnitude cheaper than whole-body clinical PET scanners, thus making the device attractive to smaller hospitals. By designing the system to perform a specific task, we can obtain better spatial resolution and sensitivity compared with conventional clinical PET scanners. This should lead to a reduction in the number of false negative scans compared with current PET technology. One issue that is often raised when proposing low cost dedicated PET

devices is the problem of tracer availability. It has been shown however that roughly 90% of the hospital beds in the U.S. are within delivery range of FDG[10], the tracer of choice for this application. This means that on-site cyclotrons will not be required for the majority of hospitals wishing to use such a device, further reducing the complexity and costs associated with the study.

Although our original proposal focused on developing a camera for axillary node imaging, on the advice of the reviewers we have broadened the scope to include direct imaging of the breast itself. One of the consequences of this was the need to make the system more flexible. It also raised some interesting questions about data acquisition strategies. Other groups proposing dedicated PET imaging systems have focussed on projection imaging or limited angle tomography, where data is acquired from just one detector position. For imaging of the axillary lymph nodes, the local geometry dictates this approach with a small camera. In the breast, however, the detectors can be rotated to give views over the full 360°, thus permitting true tomographic reconstruction. The trade-off between tomographic reconstruction and limited angle reconstruction, and the impact of statistically based reconstruction algorithms on this trade-off has been a focus of our simulation studies during the project period.

In this final report, we outline the progress made in building a dedicated PET camera (maxPET – **m**ammary and **ax**illary region PET camera) for applications in breast cancer. This includes development of the detector module, simulations of the system design, investigation into data acquisition strategies for breast imaging, development of the data acquisition hardware and software and the design and use of a realistic torso phantom.

RESEARCH REPORT

A: Detector Development

The basic detector unit consists of an array of scintillator elements coupled through a light guide into a position sensitive photomultiplier tube (PMT). Much of the work focused on evaluating different options for the PMT and on maximizing the amount of light reaching this PMT through the light guide. We chose to use the scintillator lutetium oxyorthosilicate (LSO) as the detector material because of its good stopping power, high light output and fast decay time [11] relative to bismuth germanate scintillator (the material used in the majority of clinical PET scanners). This fast decay time is of extreme importance for an axillary node or breast imaging system where only limited end shielding can be employed. The proximity of major organs such as the heart and liver which accumulate significant quantities of FDG leads to a very high singles background rate in the detectors. To avoid huge deadtime losses, it is therefore vital to use a fast scintillator such as LSO.

LSO has only recently become commercially available and supply is still somewhat limited. This has led to delays in acquiring the necessary material to build the system, and we are therefore a little way behind schedule in actually building the prototype. We recently (September 10th) took delivery of the 650 cc of uncut LSO material required to complete the prototype system. In preparation for the arrival of the LSO, we have refined our technique for accurately cutting LSO crystals using a precision diamond saw (UltraTEC, Santa Ana, CA) and have also implemented methods to achieve high light output through acid polishing of the cut crystals [12]. This process involves placing the crystals in pyro-phosphoric acid for a period of 5 minutes at 200 °C. This avoids manual polishing and saves a large amount of time and money in the detector assembly process.

We have evaluated several different photomultiplier tubes for this project, including the Philips XP1722, the Hamamatsu R5900-C8 and the Hamamatsu R5900-M64. Table 1 is a summary of the performance of these PMT's. It became clear that the Hamamatsu R5900-C8 had the best performance to cost ratio and furthermore had the advantage of being very compact and having the smallest fractional dead area. Figures 1 and 2 show the results from a prototype detector module. The module consists of an 8 x 8 array of 2x2x10 mm LSO crystals coupled through individual light guides (double clad optical fibers, Kuraray Corp., Japan) to the R5900-C8 PMT. In the flood histogram (figure 1), the 64 LSO elements are clearly resolved. The energy resolution of this module is approximately 24% (figure 2).

Table 1: Comparison of Philips XP1722, Hamamatsu R5900-C8 & Hamamatsu R5900-M64 PMT's:

PMT:	XP1722	R5900-C8	R5900-M64
structure	64 channel	4 x 4 crossed plate	64 channel
number of stages	10	11	12
gain	106 (1150V)	106 (850V)	106 (900V)
anode dark current	< 3 nA	2 nA	1 nA
pulse rise time	5 ns	1.4 ns	0.8 ns
effective area	25.4 x 25.4 mm^2	22 x 22 mm^2	18 x 18 mm^2
% active area	15%	65%	45%
cost:	~$5000	~$900	~$1700

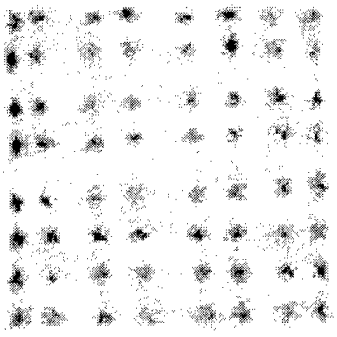

Figure 1: Flood histogram from prototype maxPET detector module. All 64 elements are clearly resolved.

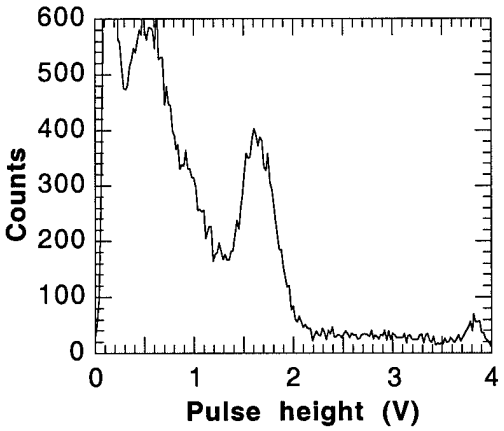

Figure 2: Energy spectrum from prototype module. Energy resolution is 24% at 511 keV

Figure 3 shows the final module design for the maxPET system. A 9 x 9 array of 3x3x20 mm crystals are coupled through 2 mm diameter optical fibers into a R5900-C8 PMT. The module measures 3 cm across and multiple modules can be packed next to each other to form an imaging plate. The module is sensitive to gamma rays right out to the edge, which means that these detectors can image very close to the chest wall. We are now proceeding to build 18 modules which will be placed into two 9 x 9 cm detector panels (3 x 3 detectors in each panel). The panels will have space to accommodate up to 5 x 5 (15 cm x 15 cm) modules to allow for future expansion.

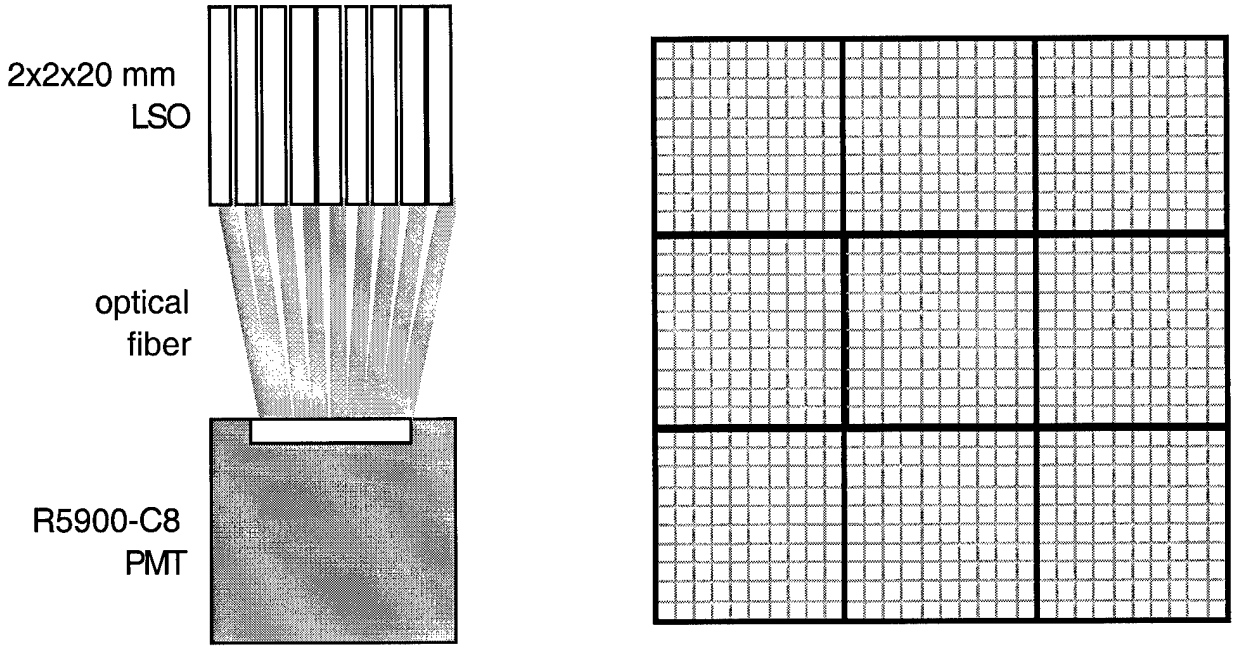

Figure 3: Drawing showing maxPET detector module (left) and panel design (right)

B: System Simulations

Introduction:

We have developed Monte Carlo simulation code and used this to examine the trade-off in a number of system design parameters (crystal size, crystal depth, plate size, plate separation). This was used to help guide the final camera design to provide a balance of high spatial resolution, high sensitivity and low cost. The simulations also allowed us to examine different reconstruction strategies, particularly for the breast imaging task, where projection, limited angle and full tomography are all options. We have also started to explore the use of statistical reconstruction algorithms on limited angle datasets in collaboration with Dr. Richard Leahy at USC and Dr. George Kontaxakis at the University of Heidelberg.

Materials and Methods:

Figure 4 shows a flow chart of the Monte Carlo code that was developed for this project. The code allows the user to set up an object containing one or more lesions. User defined parameters include

the size of the lesion, the volume of the surrounding tissue, the activity in the lesion, the activity in the background and the location of the lesion in the background. The PET camera is specified by defining the plate size, the size of the individual elements (width and depth) and the separation of the detector plates. The code is written in the C language and runs on a UNIX Sun UltraSPARC workstation (Sun Microsystems, Palo Alto, CA). Using this simulation code we have studied the complex trade-off in spatial resolution, parallax effects, sensitivity and cost [13] as it relates to the maxPET system.

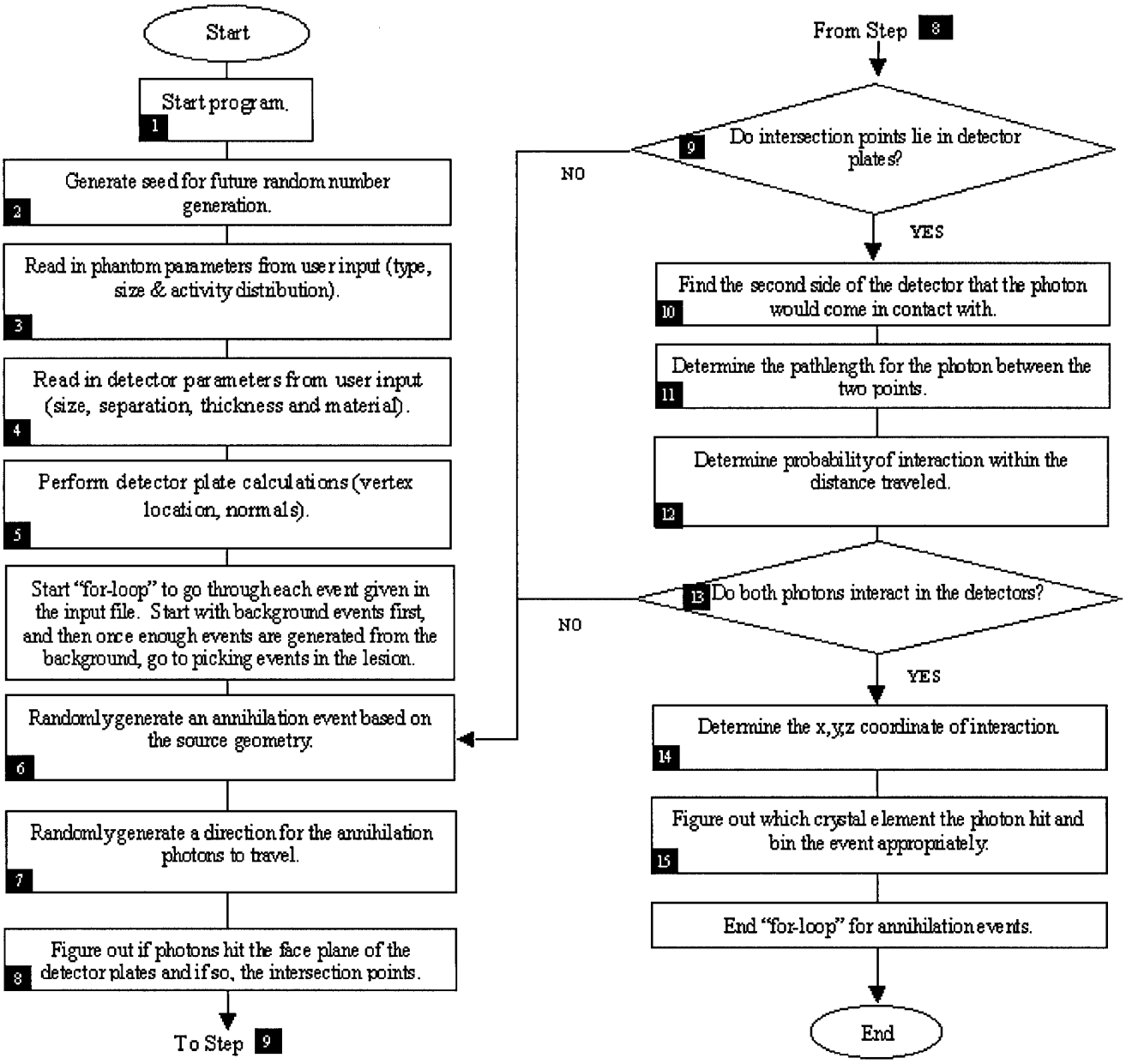

Figure 4: Flowchart for Monte Carlo simulation code.

Results:

Figure 5 shows the system sensitivity and contrast of a lesion (related to system resolution) as a function of the crystal depth, assuming 16 cm plate size, 9 cm plate separation and 2 mm cross-section LSO crystals. Notice that while the sensitivity is a very strong function of crystal depth, lesion contrast appears very insensitive. This is because resolution degradation due to parallax errors are secondary to the blurring caused by the limited angle reconstruction.

Figure 6 shows simulated images for the same geometry, but reconstructed using a range of different acceptance angles. As more angles are added in to the image, the signal to noise improves, but the outline of the breast and lesion becomes more difficult to see due to the additional blurring. Quantitative analysis however reveals that there is no significant degradation in lesion contrast relative to the surrounding background.

We are now in the process of comparing limited angle imaging with full tomography for the breast. For axillary node imaging, the system will be confined to limited angle tomography due to the geometry.

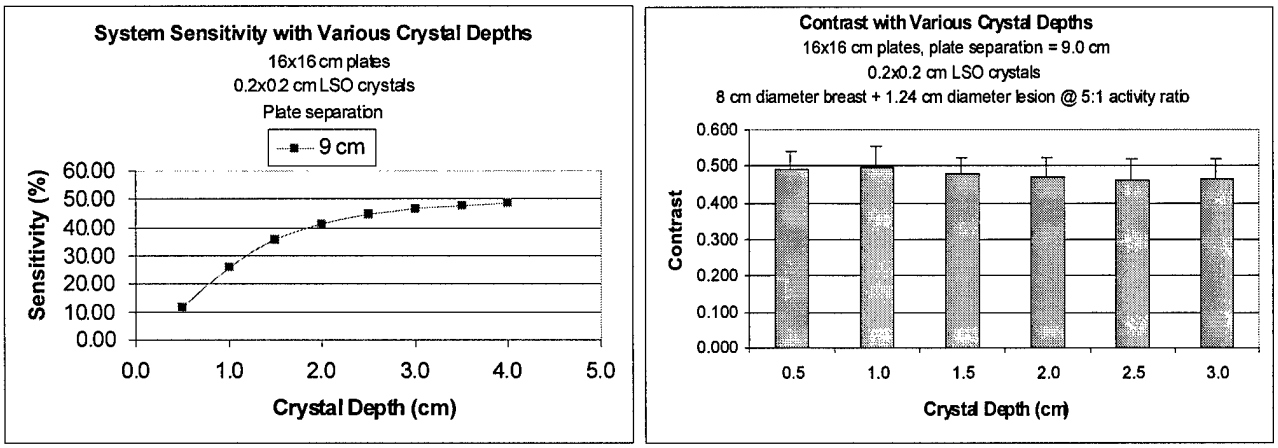

Figure 5: Simulation of system sensitivity (left) and lesion contrast (right) as a function of crystal depth. PET camera consists of two 16x16 cm plates, 9 cm apart made up of LSO crystals with 2 mm cross-section and varying depths. For the contrast simulations, the object was a 1.24 cm diameter lesion in an 8 cm diameter breast with a lesion:background activity ratio of 5:1.

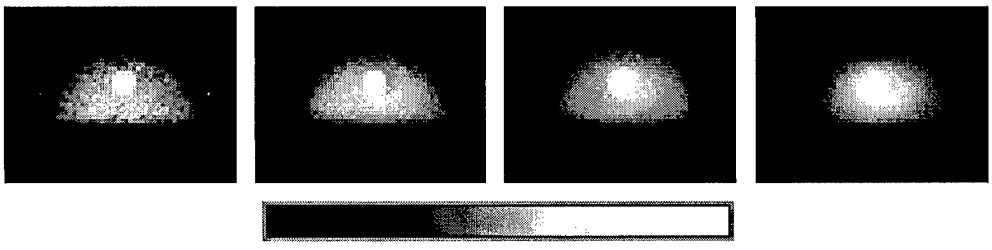

Figure 6: Simulated breast images as a function of angular acceptance angle. PET camera consists of two 16x16 cm plates, 9 cm apart made up of 2x2x20 mm LSO crystals. The simulated object was a 1.24 cm diameter lesion in an 8 cm diameter breast with a lesion:background activity ratio of 5:1.

Discussion:

Simulations have been used to measure system sensitivity and lesion contrast as system design parameters and image reconstruction strategies were varied. From this work it has become clear that the optimum LSO crystal depth is in the range of 15 – 25 mm. Crystal cross-sections of up to 3 x 3 mm allow lesions considerably smaller than 1 cc to be detected for a realistic amount of tracer in the breast. Larger plates improve sensitivity and coverage of the breast, the major limiting factor here being cost. Plate separations should be kept as small as possible to maximize sensitivity. Parallax errors are not significant when employing limited angle reconstruction. Using rotating detectors systems and filtered backprojection leads to a uniform resolution response, however this is degraded with respect to the intrinsic detector resolution due to parallax effects which contribute across the entire field of view. Preliminary results using statistical reconstruction methods suggest that the images are much less susceptible to undersampling than in the case of filtered backprojection. Acceptable tomographic images are obtained even from a single detector position. It thus may be possible to form tomographic images without rotating the detectors.

C: Data Acquisition System:

We have set up the data acquisition system to provide us with great flexibility and adequate count rate performance. Each detector plate has a set of readout electronics which will encode the position with four position sensitive signals. These eight signals (four from each plate) will be fed through a 16 channel shaping amplifier (C.A.E.N. model N568) which has an individual gain adjustment for each channel. These signals are then digitized using a 16 channel PCI board (DATEL PCI-416L) which has 12-bit A/D resolution and approximately 200 kHz rate capability (for all 16 channels). To trigger the digitizer board, the sum of the four plate outputs are fed through constant fraction discriminators and into a coincidence circuit. The output of the coincidence circuit feeds a gate and delay generator which produces the TTL pulse necessary to trigger digitization.

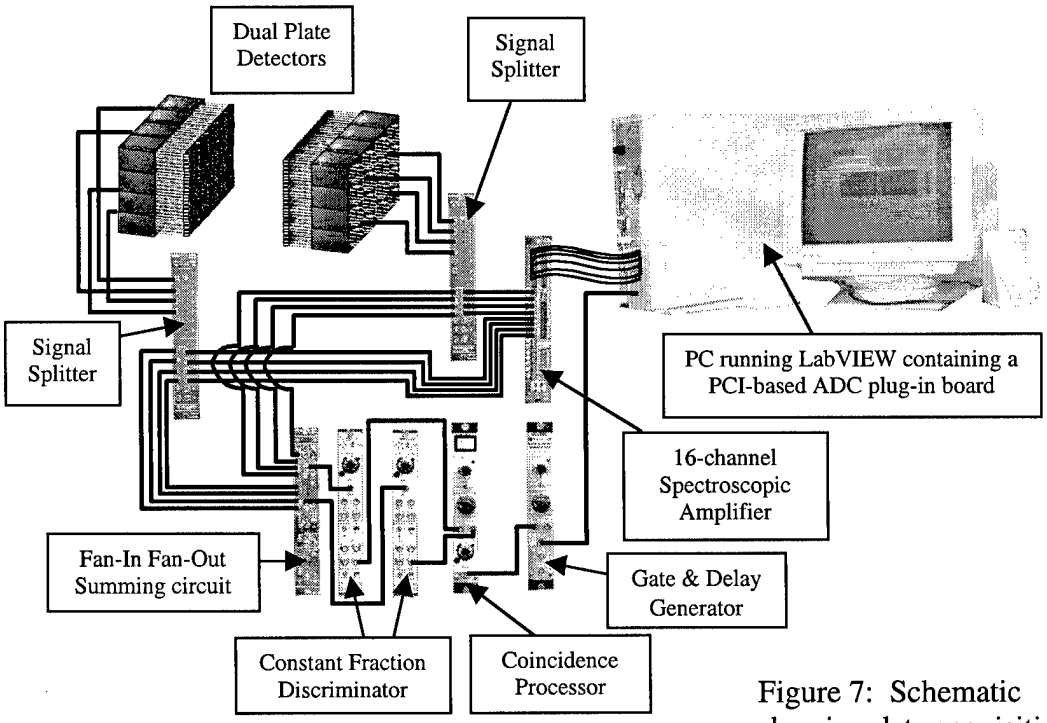

Figure 7: Schematic showing data acquisition

The host PC has a 200 MHz Pentium processor (MICRON Millenia LXE 200), 128 MB of RAM and a 4 GB hard disk for storage of raw data. LabVIEW software is used to control the data acquisition process and is also used to generate the user interface. All data will be collected in list mode with the energy stored on an event by event basis to give maximum flexibility to the subsequent reconstruction of the images. The data acquisition set-up is shown schematically in Figure 7.

D: Phantom Development:

Introduction:

Before any detector system can be tested on patients, it is vital that it go through stringent pre-clinical testing and a complete performance evaluation. Typically this is done using phantom measurements, where the phantom is a test object which can be filled with radioactivity representing to a greater or lesser extent the imaging situation in a patient. So far, most PET systems designed for breast cancer imaging applications have been tested using simple cylindrical phantoms containing one or more "hot" spheres. We feel that this can be very misleading, as the breast and axillary nodes are contained within a geometrically complex region of the body. Activity in the chest, particularly in the liver and the heart, leads to an imaging environment with a high singles to coincidence ratio and where a large fraction of events have been scattered. We have therefore developed a phantom which much more accurately represents this "hostile" imaging environment and have performed a series of experiments to show the importance of using a realistic phantom for pre-clinical testing of PET cameras for breast cancer.

Materials and Methods:

In collaboration with Radiology Support Devices, Inc. (Long Beach, CA) we have adapted a fully tissue-equivalent anthropomorphic phantom of the human thorax for axillary node and breast imaging. The phantom is constructed with tissue equivalent material with appropriate linear attenuation coefficients at 511 keV [14]. Modifications to the phantom included the addition of channels drilled in the axillary region to allow the simulation of lymph nodes using small capsules containing activity, as well as a set of breast molds in both supine and prone geometry that can be directly attached to the chest with ports for lesions and a cavity for background breast activity. In addition, the phantom contains fillable cavities accurately representing the geometry and location of the heart, liver and thoracic space, allowing the simulation of realistic background tissue uptake characteristics. Various sized-lesions may be introduced in the breast, axilla, intermammary and supraclavicular regions to simulate breast cancer patients. The dimensions of the phantom are realistically modeled after humans as shown in figure 8.
Figure 8: A photograph and schematic representation of the anthropomorphic phantom. The diagram on the right shows the physical size of the phantom.

Three different experiments were performed on a Siemens/CTI ECAT EXACT HR+ (Knoxville, TN) clinical PET scanner to demonstrate the importance of using an accurate phantom. The experiments were designed to show the role of object scatter, attenuation and activity distribution in determining signal-to-noise and contrast in images of the breast.

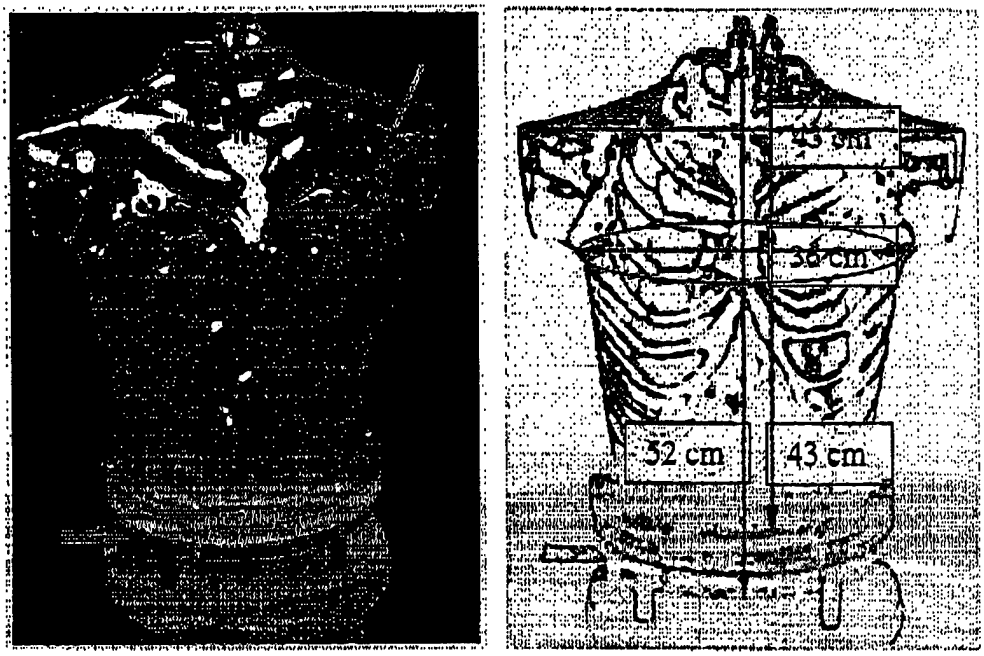

Figure 8: A photograph and schematic representation of the anthropomorphic phantom. The diagram on the right shows the physical size of the phantom.

Experiment 1: In the first experiment, supine geometry breast molds containing single lesions were scanned alone. The left breast was 514 cc containing a 2.55 cc lesion. The right breast was 456 cc and contained a 2.0 cc lesion. The lesion-to-background activities were 7:1 and 5:1 for the left and right breasts, respectively. The activity ratios were verified by taking samples and measuring them in a well counter. The breasts containing the lesions were placed in the supine position during the scanning procedure (figure 9). This setup allowed the closest simulation of a simple phantom, where the scatter and attenuation from the rest of the thorax is ignored. Also, the activity distribution is minimized to that of only the breasts and lesions alone, ignoring the thorax itself and the rest of the organs contained within.

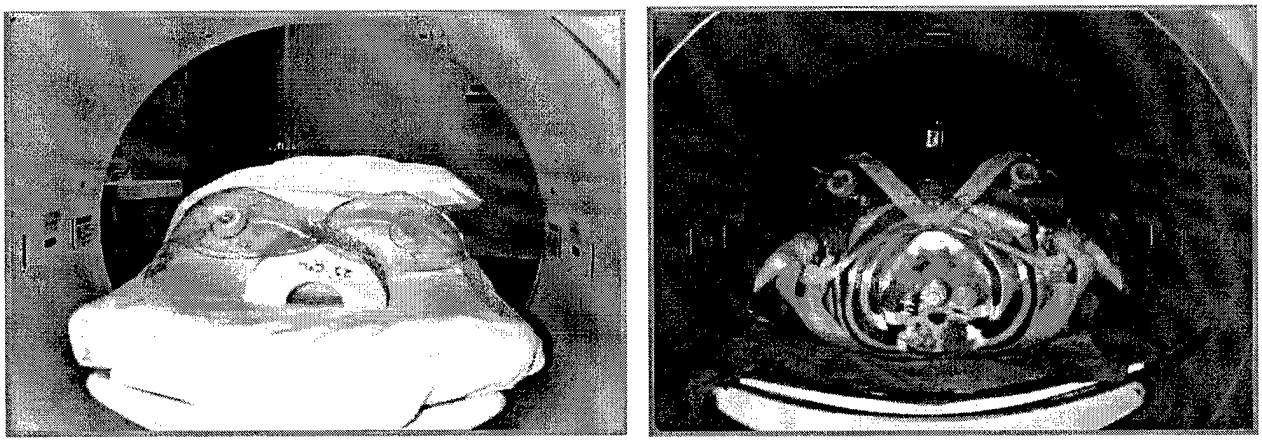

Figure 9. The picture on the left shows the breasts and lesions in the supine position in the gantry of the PET scanner as scanned in experiment 1. The picture on the right shows the position of the phantom as scanned in experiments 2 and 3.

Experiment 2: In experiment 2, the same breast molds and lesions utilized in experiment 1 were now attached to the rest of the thorax. The thorax contained the lungs, heart, and liver and was filled with cold water without any radioisotope. Again, the phantom was placed in the supine position in the scanner as shown in figure 9. In this protocol, an assessment of the contribution of attenuation and scatter only due to the presence of the thorax and its respective organs could be made. The activity distribution remained identical to that in experiment 1.

Experiment 3: In experiment 3, the thoracic cavity, heart, and liver were now all filled with realistic activity concentrations. This scanning setup provided the most complex and closest simulation to that which occurs while scanning a real patient. Thus, in this protocol, the complex geometry, attenuation, scatter and activity distribution were all replicated as closely as possible to a real human's characteristics.

In order to fill the phantom and its various components with realistic activity levels, several breast cancer patient scans from whole-body PET studies were obtained to extract the appropriate data. Regions-of-interest (ROIs) were drawn around the various tissues of interest such as the breast lesion, breast tissue, heart, liver, and background thoracic cavity using a commercially available software package (Clinical Applications Programming Package (CAPP), Siemens/CTI, Knoxville, TN). The ROI values were then converted to activity concentrations in units of microCuries per cubic centimeter for each tissue or organ and are presented in table 2.

Table 2. Concentration values for the various tissues as determined from real patient data.

Tissue/Organ	Concentration (mCi/cc) ± Std. Dev.
Lesion	0.18±0.02
Myocardium	0.13±0.02
Liver	0.11±0.007
Breast	0.05±0.006
Thoracic cavity	0.05±0.006

All the experiments followed a similar scanning protocol. The phantom was filled with ^{18}F-FDG solution as described for each experiment, based on the values in table 2. A 2-D PET scan was acquired with the breasts centered within the 15 cm axial field-of-view (FOV) and the phantom in a supine position. A 60 minute emission scan was taken right after all the components of the phantom were filled and assembled together. A 20 minute transmission scan was taken without the phantom being moved, the following morning, allowing all of the activity to have decayed more than 5 half-lives. Filtered backprojection was used for reconstructing the 63 image planes using a Shepp filter with a cutoff frequency equal to 1/2 the Nyquist frequency. No axial smoothing was performed on the images. All scans were performed on the same scanner and we maintained identical scanning conditions for each experiment.

Results:

The resulting images were analyzed using the CAPP software. ROI's were defined over the lesion and over background breast tissue. The signal-to-noise (SNR) was assumed to be proportional to the quotient of the mean ROI values of the lesion divided by the mean of the standard deviations of the background tissue ROI. The lesion ROIs were drawn on all the planes that contained lesion activity in such a fashion as to include all pixels containing at least 70% of the maximum pixel value. The background tissue ROIs were drawn on several planes of the image volume not containing any lesion activity, usually ten planes above the beginning of the lesion activity. The contrast was calculated by the mean ROI value for the lesion. Again, the same procedure for ROI drawing was used.

Figure 10 shows reconstructed images of relevant planes for each of the three experiments. One can readily see the differences in image quality due to the variation in attenuation, scatter, and activity distribution between the experimental setups as one moves from top (low scatter, no activity outside of breasts) to bottom (full scattering from thorax, activity in all organs). Figure 11 shows the calculated SNR and contrast values in each experiment. The numbers confirm the trends seen visually in the images.

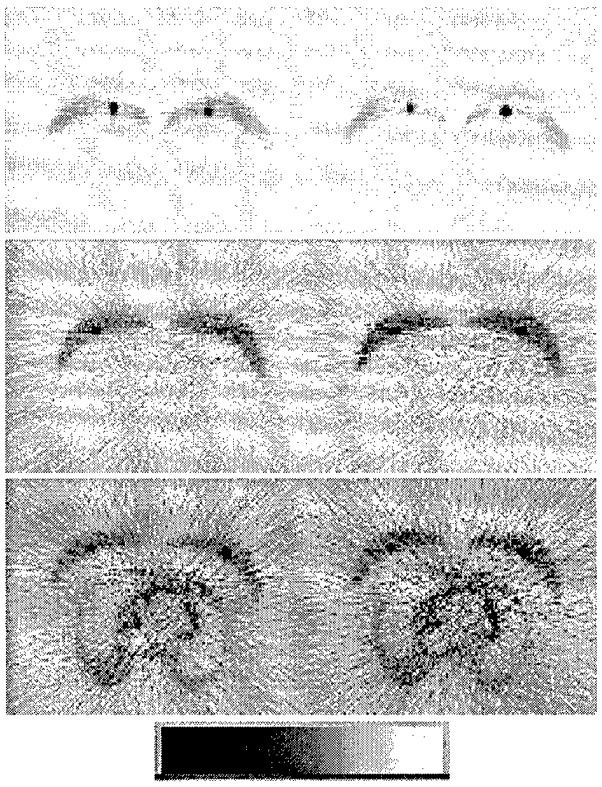

Figure 10. Images from experiment 1 (top - imaging breasts and lesions only), experiment 2 (middle - breasts and lesions attached to water-filled thorax) and experiment 3 (bottom - breasts and lesions attached to activity filled thorax). Note the change in image quality, even though the amount of radioactivity in the breast and lesions is constant through all three experiments.

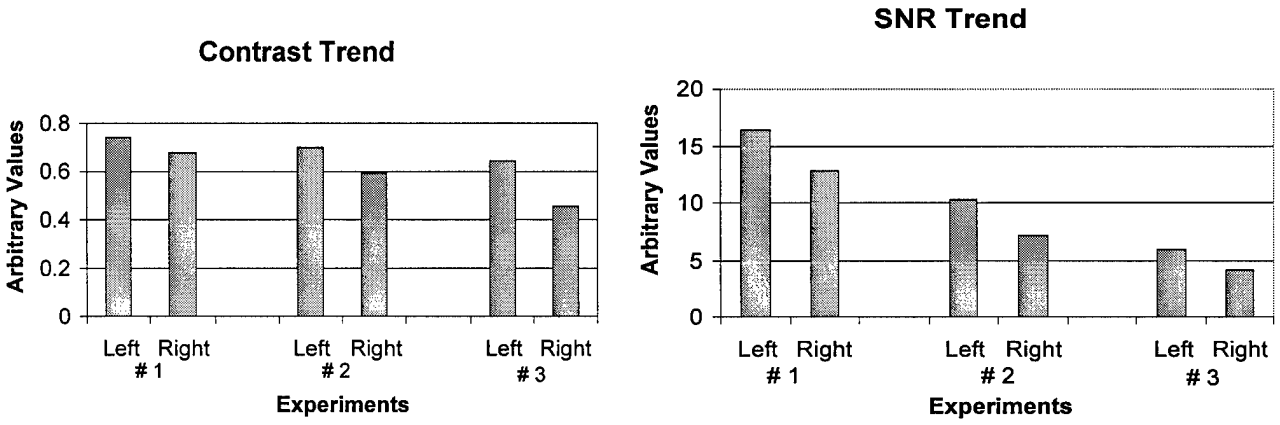

Figure 11. Graphs of the contrast and SNR trends for each of the three experiments. As scattering material and activity outside of the breasts are added, both the contrast and signal-to-noise deteriorate dramatically.

Discussion:

These experiments clearly indicate the role of attenuation, scatter and activity outside of the breast in determining image quality. Simple phantoms are likely to be insufficient when comparing imaging systems for applications in breast cancer, because they may not expose the limitations of the imaging system when operated in a hostile imaging environment. This phantom provides a way to accurately assess and optimize the performance of PET systems designed for imaging the breast and axillary nodes and will be an invaluable tool in the development and pre-clinical testing of the device currently under construction at UCLA.

CONCLUSIONS

We are close to completing a prototype PET scanner dedicated for applications in breast cancer. Detailed simulations were performed to guide the system design and all the components of the detector modules have been tested. The data acquisition hardware is in place and the acquisition code and user interface are in progress. Some delays have been experienced due to the shortage of LSO material, but with the recent delivery of LSO, we now have sufficient to build the prototype system. We anticipate the system will be completed within the next six months. The anthropomorphic phantom developed in this project will then be used to assess the prototype system and to compare its performance with other state-of-the-art PET systems.

REFERENCES

1. Danforth DN. The role of axillary lymph node dissection in the management of breast cancer. Principles and Practices of Oncology 6: 1-16 (1992).

2. Institute for Clinical PET. Clinical application and economic implications of PET in the assessment of axillary lymph node involvement in breast cancer: a retrospective study. Publication No. CE-BREAST-94.001.

3. Logager VB et al. The limited value of routine chest X-ray in the follow up of stage II breast cancer. Eur J Cancer 26: 553-555 (1990).

4. March DE et al. CT-pathologic correlation of axillary lymph nodes in breast carcinoma. J Comput Assist Tomogr 15: 440-44, 1991.

5. Niewig OE, Kim EE, Wong WH et al. Positron emission tomography with fluorine-18-deoxyglucose in the detection and staging of breast cancer. Cancer 71: 3920-25 (1993).

6. Adler LP, Crowe JP, Al-Kaisi NK, Sunshine JL. Evaluation of breast masses and axillary lymph nodes with [F-18] 2-deoxy-2fluoro-D-glucose PET. Radiology 187: 743-750 (1993).

7. Tse NY, Hoh CK, Hawkins RA et al. The application of positron emission tomographic imaging with fluorodeoxyglucose to the evaluation of breast disease. Ann Surg 216: 27-34 (1992).

8. Hoh CK, Hawkins RA, Glasby J et al. Cancer detection with whole-body PET using 2-[F-18]-fluoro-2-deoxy-D-glucose. J Comput Assist Tomogr 17: 582-589 (1993).

9. Wahl RL, Cody RL, Hutchins GD, Mudgett EE. Primary and metastatic breast carcinoma: initial clinical evaluation with PET and the radio-labeled glucose analog 2-[F-18]-fluoro-2-deoxy-D-glucose. Radiology 179: 765-70 (1991).

10. Ronald Nutt, CTI PET Systems Inc. Personal Communication.

11. Melcher CL, Schweitzer JS. Cerium-doped lutetium oxyorthosilicate: a fast, efficient new scintillator. IEEE Trans Nucl Sci 39: 505-505 (1992).

12. Huber JS, Moses WW, Andreaco MS, Loope M, Melcher CL, Nutt R. Geometry and surface treatment dependence of the light collection from LSO crystals. Nucl Inst Meth (submitted).

13. Doshi NK, Boutefnouchet A, Cherry SR. Monte-Carlo simulation of a dedicated breast and axillary node PET imaging system. J Nucl Med 39: 170P (1998).

14. Doshi NK, Basic M, Cherry SR. Evaluation of the Detectability of Breast Cancer Lesions Using a Modified Anthropomorphic Phantom. J Nucl Med 39: (1998) (to be published in November)

APPENDIX A: BIBLIOGRAPHY

Doshi NK, Basic M, Cherry SR, Pang LJ. Development of a realistic multimodality breast and axillary node phantom. J Nucl Med 38: 203P 1997 (presented at the 44th Annual Meeting of the Society of Nuclear Medicine, San Antonio, June 1997).

Shao Y, Cherry SR, Boutefnouchet A, Silverman RW, Majewski S, Wojcik R, Weisenberger AG. Evaluation of Hamamatsu R5900-M16 multi-anode PMT for readout of scintillator arrays. Presented at the 1997 IEEE Medical Imaging Conference, Albuquerque, NM, November 1997.

Boutefnouchet A, Majewski S, Cherry SR, Shao Y, Silverman RW, Meadors K, Slates R. Possibility for a very high resolution LSO PET detector based on the 16-channel R5900-M16 PMT. Presented at the 1997 IEEE Medical Imaging Conference, Albuquerque, NM, November 1997.

Doshi NK, Boutefnouchet A, Cherry SR. Monte-Carlo simulation of a dedicated breast and axillary node PET imaging system. J Nucl Med 39: 170P (1998). (presented at the 45th Annual Meeting of the Society of Nuclear Medicine, Toronto, CA, June 1998).

Doshi NK, Basic M, Cherry SR. Evaluation of the Detectability of Breast Cancer Lesions Using a Modified Anthropomorphic Phantom. J Nucl Med 39: (1998) (to be published in November)

Shao Y, Cherry SR. Depth of interaction measurement by bending optical fibers. J Nucl Med 39: 50P (1998). (presented at the 45th Annual Meeting of the Society of Nuclear Medicine, Toronto,CA, June 1998).

APPENDIX B: LIST OF PERSONNEL:

The following personnel were paid in part from this grant:

Niraj K. Doshi

Simon R. Cherry

Sanjiv Gambhir